

ON THE PERILS OF CURVE-OF-GROWTH ANALYSIS: SYSTEMATIC ABUNDANCE UNDERESTIMATES FOR THE GAS IN GAMMA-RAY BURST HOST GALAXIES

JASON X. PROCHASKA¹
Accepted to ApJ, June 19 2006

ABSTRACT

We examine the practice of deriving interstellar medium (ISM) abundances from low-resolution spectroscopy of GRB afterglows. We argue that the multi-ion single-component curve-of-growth analysis technique systematically underestimates the column densities of the metal-line profiles commonly observed for GRB. This systematic underestimate is accentuated by the fact that many GRB line-profiles (e.g. GRB 050730, GRB 050820, GRB 051111) are comprised of ‘clouds’ with a bi-modal distribution of column density. Such line-profiles may be characteristic of a sightline which penetrates both a high density star-forming region and more distant, ambient ISM material. Our analysis suggests that the majority of abundances reported in the literature are systematically underestimates and that the reported errors are frequently over-optimistic. Further, we demonstrate that one cannot even report relative abundances with confidence. The implications are profound for our current understanding on the metallicity, dust-to-gas ratio, and chemical abundances of the ISM in GRB host galaxies. For example, we argue that all but a few sightlines allow for the gas to have at least solar metallicity. Finally, we suggest new approaches for constraining the abundances.

Subject headings: gamma rays: bursts – ISM: abundances

1. INTRODUCTION

With the launch of the *Swift* satellite (Gehrels *et al.* 2004), the rate of GRB detections has increased by more than an order of magnitude (Gehrels 2006). In turn, one has seen roughly the same increase in the detection of bright afterglows. Though a few high-resolution spectra were obtained pre-*Swift* (Castro *et al.* 2003; Fiore *et al.* 2005), *Swift* has enabled the nearly routine acquisition of high signal-to-noise ratio (SNR), high-resolution spectra (Chen *et al.* 2005; Prochaska, Chen & Bloom 2006). In addition, there are now over a dozen low-resolution observations from pre-*Swift* GRB (e.g. Kulkarni *et al.* 1999; Barth *et al.* 2003) and the first year of *Swift* operation (e.g. Foley *et al.* 2005; Berger *et al.* 2005; Fynbo *et al.* 2006). Observers are now progressing toward the examination of distributions of gas properties in the interstellar medium (ISM) of GRB host galaxies.

Because of the apparent faintness of many GRB afterglows and also instrument availability, the majority of GRB spectra are acquired with low-resolution spectrometers (FWHM > 1 Å) and at moderate to poor SNR (< 50 per resolution element). In these cases, abundance analysis must be performed on the equivalent width measurements of unresolved metal-line transitions. To date, the standard practice has been to perform a multi-ion single-component curve-of-growth (MISC-COG) analysis (e.g. Savaglio, Fall & Fiore 2003) or single-component profile fits to unresolved data (e.g. Savaglio & Fall 2004; Watson *et al.* 2005) which is fundamentally the same analysis. In this analysis, one derives an effective Doppler parameter b_{eff} which principally characterizes the velocity width of strong, heavily saturated transitions. The column density is then constrained with weaker, yet still potentially saturated transitions. In contrast, the H I column density can be determined from fits to the damping wings of the

Ly α profile even with low-resolution data (e.g. Prochaska, Herbert-Fort & Wolfe 2005).

The curve-of-growth technique dates far back (e.g. Unsöld, Struve & Elvey 1930; Wilson 1939) and was primarily introduced to perform abundance analysis on lower spectral resolution data. The literature on the pitfalls of MISC-COG analysis is extensive (Nachman & Hobbs 1973; Crutcher 1975; Spitzer & Jenkins 1975). These include systematic differences in the results for ions of differing ionization state (e.g. Mg I vs. Fe II; Spitzer & Jenkins 1975), ‘hidden’ saturation due to significant variations in the Doppler parameter of overlapping components (Nachman & Hobbs 1973), and the dangers of mixing refractory and non-refractory elements (Jenkins, Savage & Spitzer 1986). The Galactic ISM community is well aware of these issues; it has taken every effort to obtain high resolution spectroscopy and when limited to low resolution data, very cautiously interpret the observations. In short, few of the problems discussed in this paper are unique to GRB research, but we note that the discussion may translate to other abundance analyses with large, modern datasets of low resolution spectroscopy (e.g. Savaglio *et al.* 2004; Turnshek *et al.* 2005).

Jenkins (1986) examined the accuracy of a single-component COG analysis on multi-component line-profiles for a range of reasonable distributions of column density and Doppler parameter. He showed that the COG results typically give results accurate to within 20% (i.e. < 0.2 dex) of the correct column density provided the N and b distributions of the individual components are well-behaved and so long as the peak optical depth $\tau_0 < 5$. Jenkins also emphasized, however, that the results would likely significantly underestimate the column densities if the N or b values were bi-modally distributed (see also Nachman & Hobbs 1973). We will find that this is frequently the case for GRB line-profiles.

In this paper, we will examine the main issues related to the ISM abundance analysis of GRB host galaxies as derived from low-resolution spectroscopy, i.e. equivalent

¹Department of Astronomy and Astrophysics, UCO/Lick Observatory; University of California, 1156 High Street, Santa Cruz, CA 95064; xavier@ucolick.org

width analysis. We begin with an analysis of the GRB 051111 sightline where Keck/HIRES observations permit one to directly test the MISC-COG technique (§ 2). The discouraging results are enlightening, namely the COG analysis systematically underestimates the column density measurements. We consider an additional example from the literature (GRB 020813) and raise similar concerns (§ 3). Finally, we offer a set of guidelines to consider when analyzing low-resolution GRB spectra (§ 4). In a future paper (Prochaska *et al.* 2006), we will apply these guidelines to our datasets and previously published results with the intent of providing a uniform, database of measurements with realistic error estimates.

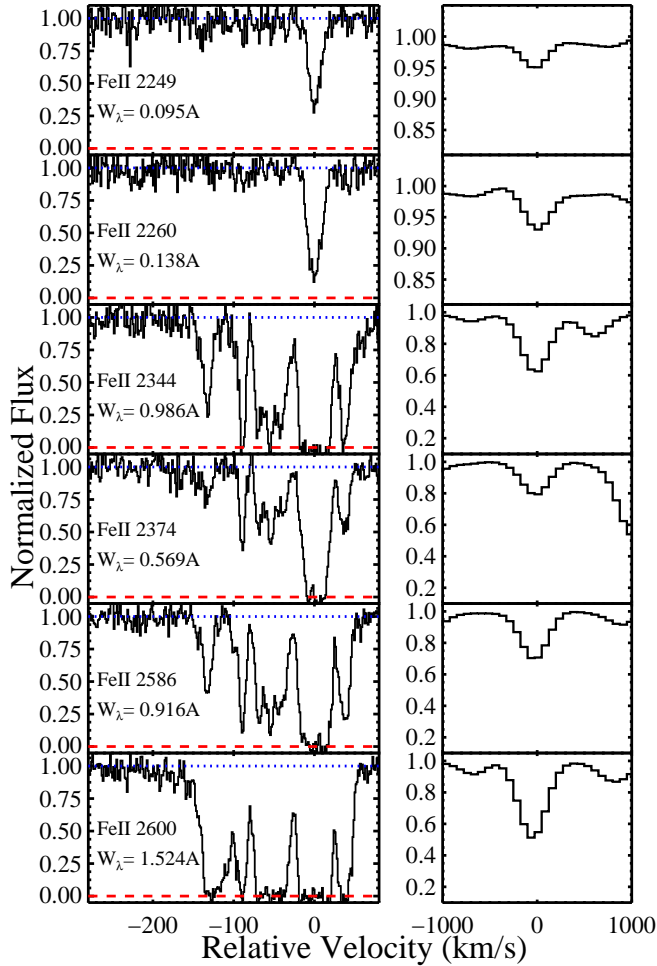


FIG. 1.— Fe II profiles from the ISM foreground to GRB 051111 in the original data (LHS) and smoothed to lower resolution (RHS; FWHM $\approx 5\text{\AA}$) to mimic the line-profiles frequently observed. The velocity $v = 0$ corresponds to $z = 1.54948$. The rest equivalent width values labeled on the Figure correspond to the full line-profile.

2. GRB 051111: A TEST CASE

To illustrate the key issues related to deriving abundances from equivalent width measurements, we will examine a GRB sightline where the column densities are well-constrained, i.e., an afterglow with high quality, high resolution observations. The Keck observatory staff acquired HIRES (Vogt *et al.* 1994) observations of the bright afterglow of the $z \approx 1.55$ GRB 051111 (Hill *et al.* 2005)

at high spectral resolution FWHM $\approx 6\text{ km s}^{-1}$ and moderate signal-to-noise ratio (≈ 7 per 1.3 km s^{-1} pixel) and released the data to the public². The data reveal the detection of over 50 transitions (Prochaska *et al.* 2006) including a wealth of fine-structure levels (Prochaska, Chen & Bloom 2006). Our treatment begins with a single-component COG analysis of the Fe⁺ ion and then proceeds to a MISC-COG analysis of other ions in the ISM surrounding GRB 051111.

TABLE 1
EQUIVALENT WIDTH MEASUREMENTS FOR
GRB 051111

Ion	J^a	λ (\AA)	$\log f$	W_λ^b (m \AA)	N_{adopt}^c (cm^{-2})	τ_0^d
Ni II		1709.604	-1.4895	54.2 ± 7.2	13.97	1.1
		1741.553	-1.3696	76.6 ± 6.8		1.5
		1751.916	-1.5575	48.5 ± 6.8		1.0
Mg I		1747.794	-2.0419	72.3 ± 6.1	14.68	1.6
		1827.935	-1.6216	133.3 ± 5.9		4.5
		2026.477	-0.9508	279.7 ± 4.3		23.2
Si II						
Zn II	1/2	1808.013	-2.6603	338.4 ± 7.8	> 16.14	> 11.7
		2026.136	-0.3107	237.9 ± 4.4	> 13.71	> 10.9
Cr II		2062.664	-0.5918	176.7 ± 5.0		> 5.8
		2056.254	-0.9788	154.9 ± 5.1	13.88	3.5
Fe II		2066.161	-1.2882	88.8 ± 5.5		1.7
	9/2	2249.877	-2.7397	112.9 ± 6.8	15.32	1.8
	9/2	2260.780	-2.6126	155.1 ± 6.5		2.5
	9/2	2344.214	-0.9431	985.6 ± 9.5		120.0
	9/2	2374.461	-1.5045	569.0 ± 7.9		33.4
	9/2	2586.650	-1.1605	916.4 ± 7.9		80.2
	9/2	2600.173	-0.6216	1523.8 ± 7.8		279.0
Fe II	7/2	2333.516	-1.1601	205.9 ± 4.3	14.01	3.5
	7/2	2396.356	-0.5414	405.8 ± 4.9		15.0
Mn II		2576.877	-0.4549	260.6 ± 5.1	> 13.64	> 8.5
		2594.499	-0.5670	229.5 ± 4.1		> 6.6
		2606.462	-0.7151	213.2 ± 5.3		> 4.7

^a J value for ions with excited states.

^bRest equivalent width.

^cWeighted-mean value.

^dPeak optical depth of the line profile assuming the column density from Column 6 and $b = 7\text{ km s}^{-1}$.

2.1. Single-component COG Analysis

We will focus first on the Fe II transitions (Figure 1) from the ground-state ($J = 9/2$) level and will adopt the Fe⁺ column density $N(\text{Fe}^+) = 10^{15.27 \pm 0.01} \text{ cm}^{-2}$ from Prochaska, Chen & Bloom (2006). We have measured the total rest equivalent width of each Fe II transition and its associated statistical uncertainty (Table 1). At the resolution and signal-to-noise of these HIRES data, the rest equivalent width statistical uncertainty at 6000 \AA in one pixel is $\sigma(W_\lambda) = 1.5\text{ m\AA}$. To better match the low resolution observations, consider an analysis assuming total

²<http://www.graasp.org>

uncertainty $\sigma(W_\lambda) = 30\text{mÅ}$. Figure 2 presents a single-component COG analysis of the Fe II transitions which is a two parameter fit to the data: the column density N_{best} and the effective Doppler parameter b_{eff} . The upper panel shows the reduced equivalent widths W_λ/λ plotted against the $f\lambda$ product. The single-component model which minimizes χ^2 is overplotted on the observations. The model is driven to match the high W_λ transitions because for fixed $\sigma(W_\lambda)$ these measurements have the highest relative SNR. This is a generic result for the analysis of unresolved line-profiles. The lower panel presents the $\Delta\chi^2$ contours for the N, b_{eff} parameter space. The best-fit model (and its 2σ error ellipse) underestimates the correct total Fe⁺ column density by 0.6 dex, i.e. a factor of 4.

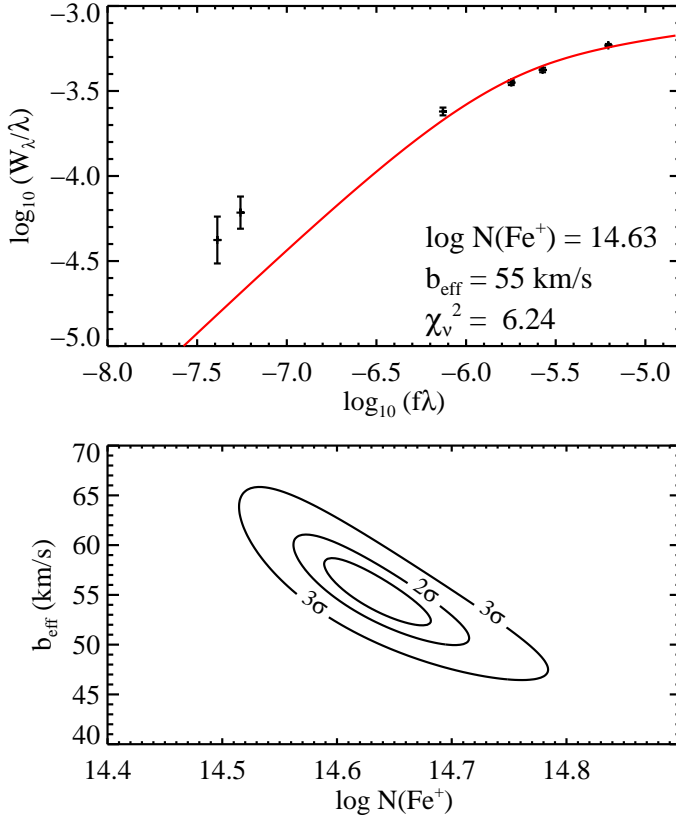


FIG. 2.— Single-component COG analysis of the Fe II transitions for GRB 051111 under the assumption that the equivalent width error $\sigma(W_\lambda) = 30\text{mÅ}$ for each transition. The upper panel presents the W_λ measurements and the model which minimizes χ^2 . The lower panel shows $\Delta\chi^2$ contours for the b_{eff}, N parameter space. The best-fit column density (and 2σ error ellipse) severely underestimate the true column density $N_{true} = 10^{15.24} \text{ cm}^{-2}$.

Why does the single-component COG model systematically underestimate the Fe⁺ column density? The principal reason is that a single-component line-profile is only a good representation of the two weakest Fe II transitions (Figure 1). In order to match the observed equivalent width of the strong Fe II transitions which are comprised of many (> 10) ‘clouds’, a single-component COG analysis is driven to a large effective Doppler parameter, i.e. $b_{eff} > 50 \text{ km s}^{-1}$. The only physical significance of this large b_{eff} value is that it describes the total velocity width of the very strongest lines ($\Delta v \approx 200 \text{ km s}^{-1}$).

For this sightline, over 90% of the Fe⁺ ions are associated with the component at $v = 0 \text{ km s}^{-1}$ and confined to $\Delta v \approx 20 \text{ km s}^{-1}$. Meanwhile, the gas responsible for $> 80\%$ of the equivalent width accounts for less than 10% of the total column density. It is this bi-modality in component column densities and the inclusion of highly saturated transitions which leads to such poor results for the COG analysis.

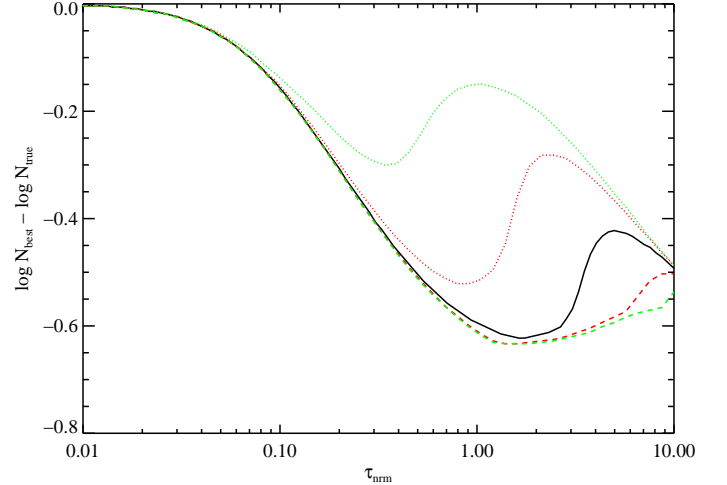


FIG. 3.— Offset between the best-fit column density N_{best} for a single-component COG analysis and the true column density N_{true} . In this analysis, we have adopted the Fe⁺ optical depth profile from the unsaturated regions of the Fe II 2260, 2374, and 2586 transitions for GRB 051111. We then varied the normalization of the optical depth profile τ_{nrm} , measured the W_λ values for each of the transitions in Figure 1, and minimized χ^2 for N_{best} and b_{eff} . The solid curve shows the offsets assuming $\sigma(W_\lambda) = 0.03\text{mÅ}$ for each transition. The dotted curves show the results assuming $\sigma(W_\lambda)$ is twice and four times smaller for the weakest transitions (Fe II 2249 and 2260). Finally, the dashed lines show the results assuming $\sigma(W_\lambda)$ is $2\times$ and $4\times$ larger for the weakest transitions.

The best-fit N_{best} value is sensitive to the error estimate $\sigma(W_\lambda)$ that we adopt, although only if we alter the *relative* uncertainty. For example, if we set $\sigma(W_\lambda) = 40\text{mÅ}$ for each transition then we will derive the same results as in Figure 2, albeit with a larger error ellipse. This is because, the relative χ^2 of each line is unaltered. If we instead we increase $\sigma(W_\lambda)$ for only the strongest transitions, the best-fit model slowly approaches the correct value. Figure 3 describes these trends. For this Figure, we have first derived the optical depth profile of the Fe⁺ gas by combining the unsaturated observations of the Fe II 2260, 2374, and 2586 profiles. We then varied the normalization of the optical depth profile ($\tau_{nrm} = 1$ corresponds to the data as observed), measured the equivalent widths of the transitions, and minimized χ^2 to derive N_{best} and b_{eff} . The solid curve shows the results assuming $\sigma(W_\lambda) = 30\text{mÅ}$ for each transition. At small τ_{nrm} , the transitions are optically thin and one recovers the correct result independent of the best-fit b_{eff} value. At $\tau_{nrm} > 1$, the N_{best} value is systematically lower than N_{true} . The dotted curves in the Figure show the results when we reduce the uncertainty in the Fe II 2249, 2260 transitions by a factor of 2 and 4 respectively. This leads to a significant improvement

for $\tau_{nrm} < 5$ where the lines are at most modestly saturated. The dashed lines show the results where $\sigma(W_\lambda)$ is increased by 2 and 4 times for the weak transitions. The key conclusions to be drawn from Figures 2 and 3 is that the standard single-component COG analysis may lead to a severe underestimate of the gas column density.

There are three signatures that the single-component COG analysis is providing an underestimate of the column density. First, the effective Doppler parameter exceeds 50 km s^{-1} . Low-ion line-profiles in the Galactic ISM (e.g. Spitzer & Fitzpatrick 1995; Howk, Savage & Fabian 1999), damped Ly α systems (e.g. Prochaska & Wolfe 1996; Dessauges-Zavadsky *et al.* 2003), and GRB sightlines (e.g. Chen *et al.* 2005) all break into individual components with Doppler parameters $b < 20 \text{ km s}^{-1}$. This is especially true for the cloud which corresponds to the peak optical depth of the line. On its own, however, the derivation of a large b_{eff} value does not require that the measurement is erroneous Jenkins (1986). But, if one adopts $b_{eff} \gg 20 \text{ km s}^{-1}$ then *one will calculate column densities for weaker transitions in the optically thin limit even if these transitions are actually saturated*. A second signature is that the reduced χ^2_ν is large. This is likely to be a universal result for GRB observations, again because the single-component model is a poor representation of the data. The key concern here is that the error estimate that one derives from a $\Delta\chi^2$ analysis will generally be far too optimistic. Finally, the most important signature is when the reduced equivalent width of the weakest transitions are significantly under-predicted by the model. This is the most striking feature in Figure 2. We note that this effect is also evident, for example, in the Fe⁺ measurements for GRB 000926, GRB 010222, and GRB 050505 as analyzed by Savaglio, Fall & Fiore (2003) and Berger *et al.* (2005).

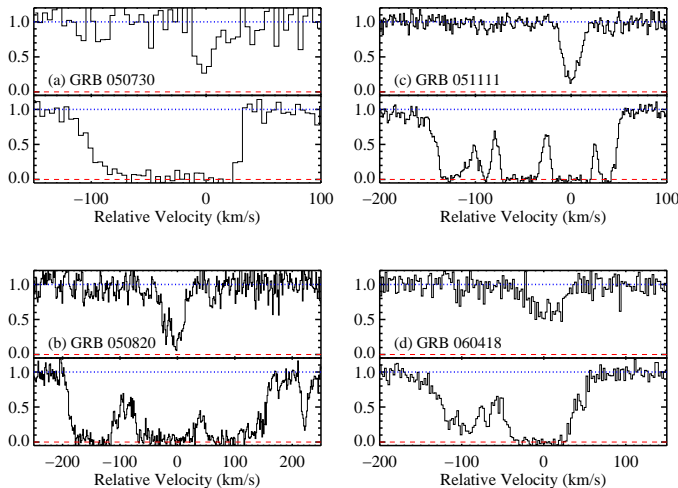


FIG. 4.— Velocity profiles for a weak and strong transition arising in the ISM of the host galaxies of (a) GRB 050730, (b) GRB 050820, (c) GRB 051111, and (d) GRB 060418 (Prochaska *et al.* 2006). Note that the majority of column density is associated with a single, narrow component whereas the equivalent width of the strongest transitions is dominated by weaker ‘clouds’. It is this bi-modal aspect of the column density distribution which accentuates the failings of the single component COG analysis.

Before proceeding to the multi-ion, single-component COG analysis, we wish to comment on our results in light of the analysis by Jenkins (1986). As noted in the Introduction, Jenkins (1986) warned that the single-component COG analysis would significantly underestimate the column density in cases where the optical depth distribution for the individual components is not smoothly distributed (i.e. bi-modal). Indeed, this is the case for the line-profiles for GRB 051111 (Figure 1). We emphasize that this is also the case for the ISM gas associated with GRB 050730 and GRB 050820, i.e. every case where moderate SNR, high-resolution echelle data exists (Chen *et al.* 2005; Prochaska *et al.* 2006). Again, the total optical depth of the line-profiles is dominated by a single, narrow component and the total equivalent width (for strong transitions) is dominated by low column density clouds. We expect that a bi-modal distribution of N values will be characteristic of many GRB sightlines³: the high column density component may be related to the surrounding star-forming region and the lower column density gas may arise from the ambient ISM or even halo of the galaxy. Figure 4 compares one weak and one strong transition from the ISM of the host galaxies of GRB 050730, GRB 050820, GRB 051111, and GRB 060418 (Prochaska *et al.* 2006). It is evident that the majority of column density is in a single narrow component while the equivalent width is dominated by multiple, weaker components. Of course, additional high-resolution observations of GRB afterglows will help reveal the typical N and b distributions of the line-profiles.

2.2. Multi-ion Single-component COG Analysis

Let us now consider a multi-ion single-component COG (MISC-COG) analysis for the GRB 051111 transitions. To date, this has been the standard approach for analyzing low-resolution GRB spectra. In this analysis, one minimizes the global χ^2 for a single b_{eff} value and unique N_{best} values for each ion considered. Figure 5 shows the results for a number of ions observed toward GRB 051111. As before, we have assumed $\sigma(W_\lambda) = 30 \text{ mÅ}$ for all of the transitions. Aside from the weakest Mg I and Fe II transitions, we find the data is reasonably well represented by this model, primarily because each ion has an additional degree of freedom associated with it. In fact, one could easily choose to ignore the ‘discordant’ Mg I and Fe II points on account of line-blending and/or an unidentified cosmic-ray (especially if the observations include only one or two examples). We emphasize, however, that these data points are severely discrepant because (i) the analysis includes at least one strong, heavily saturated transition ($\tau_0 > 5$) from each ion which has driven N_{best} to a systematically low value; and (ii) the transitions are optically thin and therefore highlight that the N_{best} value is too low.

The lower panel of Figure 5 shows the offset between N_{best} and N_{true} for each of the ions. The effects for Si⁺, Zn⁺, and Mn⁺ are expressed as upper limits (i.e. the offset is at least as large as indicated) because the N_{true} values derived from the HIRES observations are conservative lower limits due to line saturation. It is evident that the abundances for all of the ions are systematically un-

³In passing, we also note that a bi-modal column density distribution is also characteristic of many of the damped Ly α systems (e.g. Prochaska *et al.* 2001).

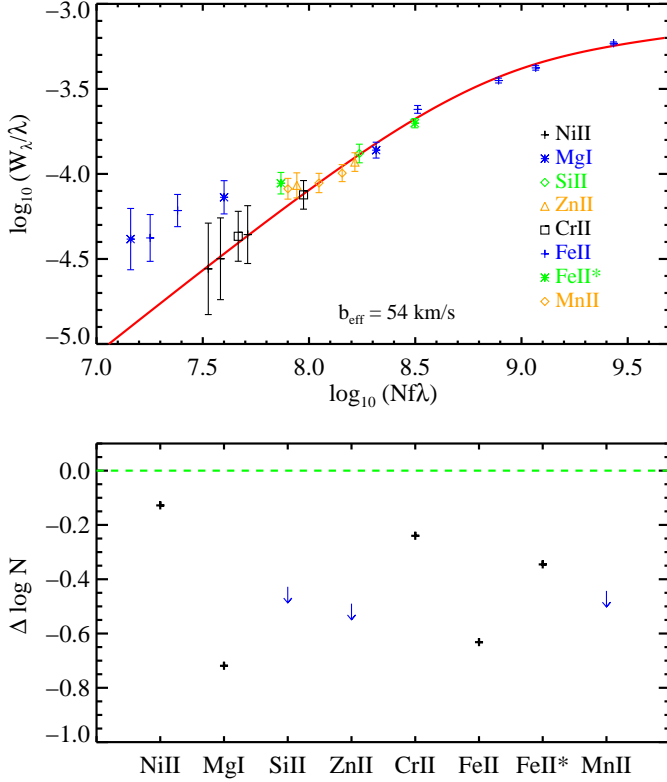


FIG. 5.— The multi-ion single-component curve-of-growth (MISC-COG) analysis for a series of ions observed in the ISM of GRB 051111. The upper panel shows the best-fit model and the observations. The lower panel shows the offset for the best-fit column density and the actual value. The arrows indicate lower limits to the offsets because the Si II, Zn II, and Mn II transitions are all saturated at echelle resolution.

derestimated with offsets of 0.15 dex to at least 0.7 dex. The case of Zn^+ is particularly problematic. The measurements consist of two Zn II transitions with $f\lambda$ values that differ by 0.3 dex. The observations are well fit by the MISC-COG analysis yet $N(\text{Zn}^+)_{\text{best}}$ is at least 0.5 dex too low. The explanation is relatively simple: the effective Doppler is so large that these saturated profiles are treated as if they lie on the linear portion of the COG, i.e.,

$$N = \frac{W_\lambda}{\lambda} \frac{1.1 \times 10^{20} \text{ cm}^{-2}}{f(\lambda/\text{\AA})} \quad (1)$$

with λ in Angstroms. To summarize, the analysis is driven by the strong Fe II transitions to a large b_{eff} value which leads to a systematic underestimate of the column density of all the ions. As worrisome, the underestimate varies from ion to ion and one cannot even calculate relative abundances to uncertainties of less than 0.3 dex.

Not surprisingly, the results are improved if one eliminates the four strongest Fe II transitions from the analysis (Figure 6). We find, however, that we still derive a b_{eff} value that is too large and therefore significantly underestimate the column densities of several of the ions. If we only include those transitions which are unsaturated at echelle

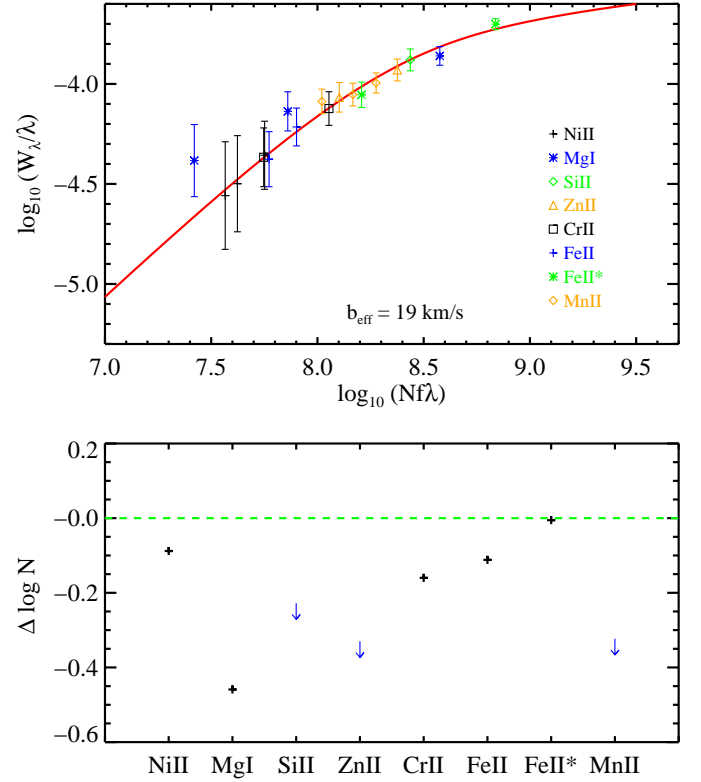


FIG. 6.— Same as Figure 5 except we have removed the strongest Fe II transitions from the analysis. The results are significantly improved due to the lower b_{eff} value, yet the column densities of Mg I, Si II, Zn II, and Mn II are still significantly underestimated.

resolution⁴ (i.e. consider only those lines which are truly on the linear portion of the COG), one finally achieves reasonable results. With low-resolution spectroscopy, however, one does not have this luxury. We are particularly worried that low-resolution spectroscopy is generally limited to the analysis of transitions with $\log(W_\lambda/\lambda) > -4$.

3. GRB 020813: A HIGH SNR, LOW-RESOLUTION EXAMPLE FROM THE LITERATURE

Let us now consider a low-resolution spectroscopic example from the literature, GRB 020813. Barth *et al.* (2003) obtained a high signal-to-noise, low-resolution spectrum of this afterglow with the LRIS spectrometer (Oke *et al.* 1995) in spectropolarimetry mode. Barth *et al.* (2003) reported equivalent width measurements for many transitions associated with the ISM surrounding GRB 020813. We present in Figure 7 a single-component COG analysis of the Fe II transitions detected in their data. Similar to GRB 051111 (Figure 2), the strong transitions drive the best-fit model to a large b_{eff} value. In contrast to GRB 051111, however, the weak Fe II 2249 and Fe II 2260 transitions are well-modeled by this fit. The error ellipse for this model indicates a very precise measurement, $N(\text{Fe}^+) = 10^{15.52 \pm 0.03} \text{ cm}^{-2}$, in good agreement with the line-profile analysis of Savaglio & Fall (2004). The correspondence between the two analyses does not lend additional confidence; for unresolved features, a single-component

⁴This does not include Si^+ or Zn^+ whose lines have $\tau_0 > 5$.

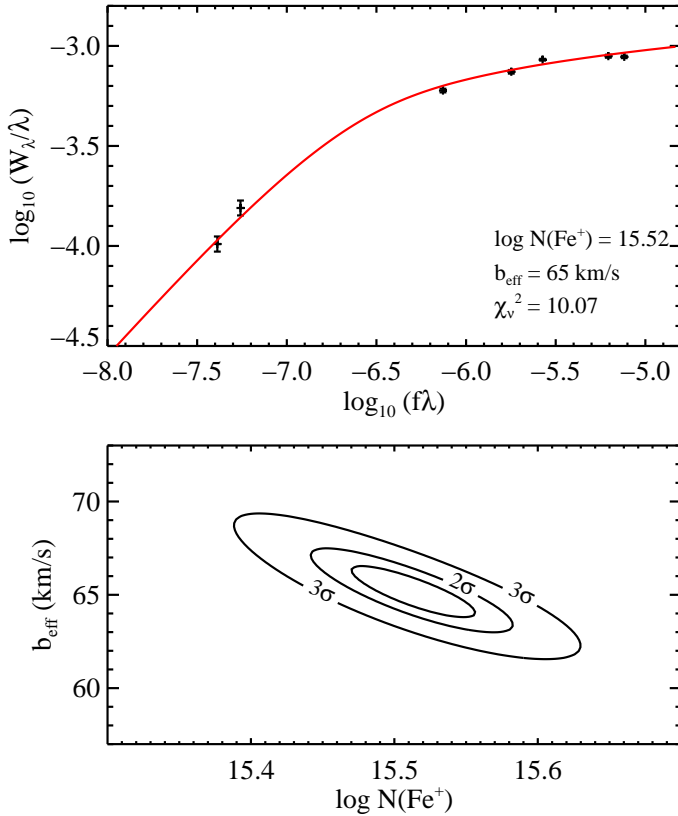


FIG. 7.— Single-component COG analysis of the Fe II transitions for GRB 020813. The upper panel presents the W_λ measurements and the model which minimizes χ^2 . The lower panel shows $\Delta\chi^2$ contours for the b_{eff} , N parameter space (note the tiny dynamic range).

line-profile analysis is identical to the COG method.

Because of the good visual agreement of the model (formally the χ^2_ν value is very poor) and the very small error ellipse, one is led to believe that the column density has been precisely determined. This is an incorrect conclusion. First, consider the best-fit value $N_{\text{best}} = 10^{15.52} \text{ cm}^{-2}$. Adopting $b_{\text{eff}} = 65 \text{ km s}^{-1}$, the line-profile of the Fe II 2249 and 2260 transitions are optically thin, i.e. the transitions are predicted to lie on the linear portion of the COG (Figure 7). In this case, one can calculate $N(\text{Fe}^+)$ from Equation 1 and find values of $10^{15.45} \text{ cm}^{-2}$ and $10^{15.50} \text{ cm}^{-2}$ for Fe II 2249 and 2260 respectively. While this result appears to be self-consistent, consider the implication: the rest equivalent widths of these two transitions are very large, in fact $2.5\times$ larger than the partially saturated Fe II transitions for GRB 051111 (Figure 1). To account for these large equivalent widths and the best-fit column density, one must hypothesize a line-profile consisting of a series of non-overlapping components that have large column density, but not too large ($N \sim 10^{15} \text{ cm}^{-2}$). While this cannot be ruled out by the observations, we consider this scenario to be highly unlikely in light of the observed line-profiles of GRB sightlines at high-resolution (e.g. Figure 1).

To emphasize this point, consider Figure 8 where we compare the single-component scenario with an alternate model. The profiles on the left-hand side show several of the observed Fe II transitions predicted by the best-fit

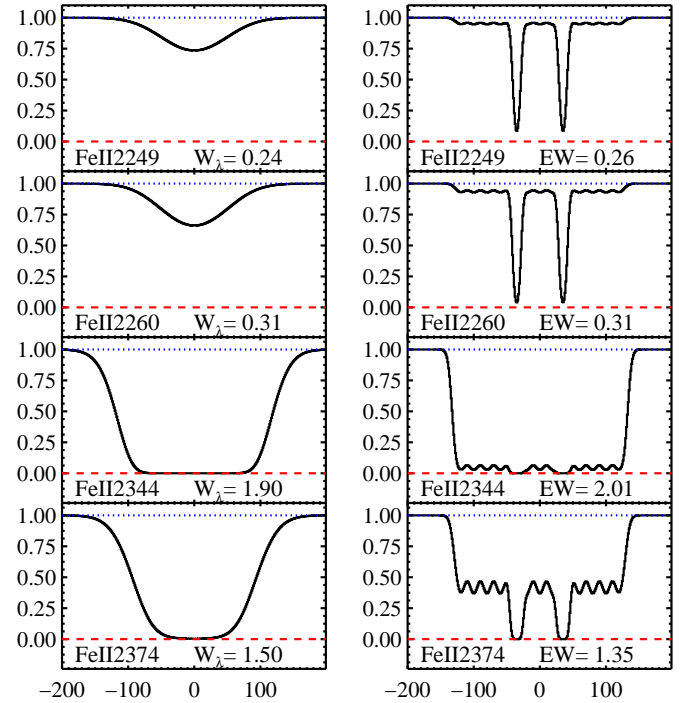


FIG. 8.— Model profiles for the Fe II transitions of GRB 020813. The LHS shows the single-component profile corresponding to the best-fit model for Figure 8. Note that the two Fe II transitions are optically thin even though they exhibit relatively large W_λ values. The RHS shows a toy model of the line-profile consisting of two strong, narrow components and a series of weak features. It presents a good match to the observed equivalent widths yet has 100% higher column density than the single-component model.

model. The right-hand side shows a toy model consisting of two strong, narrow components (each with $\log N = 15.4$ and $b = 5 \text{ km s}^{-1}$) and a series of weak components included to reproduce the large equivalent width of the stronger Fe II transitions. This toy model provides a reasonable match to the observed equivalent widths (in fact, a better fit to the strong transitions) and implies a total Fe^+ column density that is two times larger (0.3 dex or 10σ) than the single-component COG result.

We do admit, however, that it may be difficult to construct an optical depth profile for GRB 020813 where the true Fe^+ column density is $10\times$ larger than the single-component COG value. And, we note that the low SNR, high-resolution VLT/UVES observations of GRB 020813 (Fiore *et al.* 2005) do suggest that the optical depth profile is not dominated by only a single strong component. Nevertheless, we consider it impossible that the best-fit COG value is not underestimating the $N(\text{Fe}^+)$ value. Furthermore, we are certain that the statistical error estimate grossly underestimates the systematic uncertainty associated with one's assumptions about the optical depth profile.

Continuing with the treatment of GRB 020813, Figure 9 presents the MISC-COG analysis for a series of the ions detected in the Barth *et al.* (2003) spectrum. Again, the model is visually a good fit to the observations and we derive column densities that are in good agreement with Savaglio & Fall (2004). The issues that exist for Fe^+ are accentuated for the Si^+ and Zn^+ results. Here, the

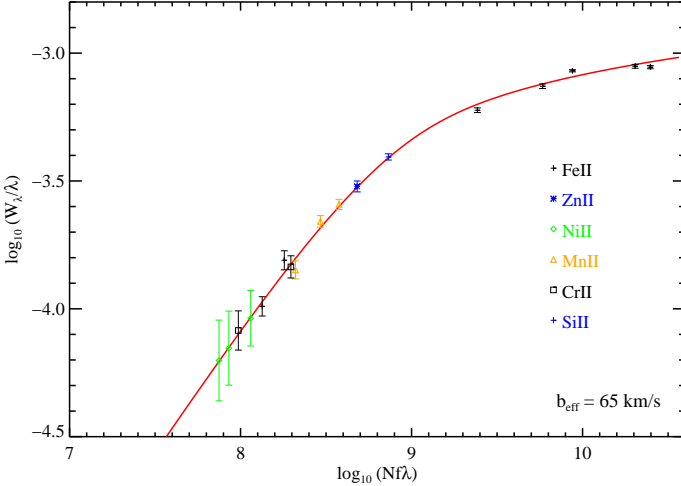


FIG. 9.— MISC-COG analysis of the ions in the ISM of GRB 020813. Because of the large b_{eff} values demanded by the heavily saturated Fe II transitions, the other transitions are treated as if they lie on the linear portion of the curve-of-growth. This leads to unrealistically low central values for the best-fit column densities and overly optimistic error estimates.

rest equivalent widths are $W_\lambda = 0.7\text{\AA}$ and 0.6\AA for the Si II 1808 and Zn II 2026 profiles, i.e. very large. Yet, again, the best-fit column densities correspond to the optically thin limit because of the large b_{eff} value. It is nearly impossible to construct optically thin Si II 1808 and Zn II 2026 line-profiles if one is restricted to physically realistic individual clouds with $b < 10\text{ km s}^{-1}$. Furthermore, *there is no observational constraint which sets an upper limit to the Si^+ and Zn^+ column densities.*

These are generic results for any MISC-COG analysis that gives a very large b_{eff} value: the technique models transitions with very large equivalent width measurements as being optically thin and adopts the lowest column density conceivable. The bottom line is that one is very likely to underestimate the column densities of all of these ions. And, the error estimates should reflect a one-sided distribution allowing only significantly larger values, i.e. lower limits.

4. CONSERVATIVE SUGGESTIONS FOR EQUIVALENT WIDTH ANALYSIS

Given the cautionary (pessimistic) tone of the previous sections, one may draw the conclusion that no progress on chemical abundances can be made with low-resolution GRB spectroscopy. To push forward in a productive yet cautious manner, we offer the following suggestions.

1. Assume that every line-profile is saturated and examine all possible constraints to demonstrate otherwise. Absent additional constraints, the equivalent width measurements establish only lower limits to the column densities.

2. Consider independent analyses of the heavily saturated and the weakest lines. The former may give estimates for the abundances of the ambient ISM along the sightline while the former could be more relevant to the gas near the star-forming region. Unfortunately, one cannot separate the H I gas along the sightline into these

two phases so the goals of such analysis would be to (i) prevent the strong strong lines from biasing the total column density to low values and (ii) attempt to measure relative abundances in the two ‘phases’. We reemphasize that by considering one COG analysis for all the lines, the strong lines will drive the COG analysis to large b_{eff} values which forces the column densities of weaker (yet likely saturated) transitions to their minimum value. The end result is a systematic underestimate of all column densities. A corollary to this suggestion is that the results for a single-component COG analysis with $b_{eff} > 20\text{ km s}^{-1}$ are highly suspect.

TABLE 2
WEAK LINES FOR UPPER LIMITS

Transition	λ (\AA)	$\log f$	$N_{\tau_0=2}^a$ (cm^{-2})	W_λ^b (m \AA)	$[\text{M}/\text{H}]^c$
SiII 1250	1250.5840	−2.2634	15.29	82	−1.91
OI 1355	1355.5977	−5.9066	18.90	89	0.16
BII 1362	1362.4611	−0.0057	13.00	90	0.21
NiII 1467b	1467.7560	−2.0044	14.96	97	−1.29
PII 1532	1532.5330	−2.1186	15.06	101	−0.47
GeII 1602	1602.4863	−0.8428	13.76	106	0.13
FeII 1611	1611.2004	−2.8665	15.79	106	−1.71
NiII 1703	1703.4050	−2.2218	15.12	112	−1.13
MgI 1747	1747.7937	−2.0419	14.93	115	−2.65
FeII 1901	1901.7729	−3.9961	16.84	125	−0.66
CrII 2066	2066.1609	−1.2882	14.10	136	−1.57
FeII 2249	2249.8767	−2.7397	15.51	148	−1.99
SiII 2335	2335.1230	−5.3716	18.13	154	0.57
TiII 3230	3230.1311	−1.1630	13.78	213	−1.16

^aColumn density corresponding to a line-profile with peak optical depth $\tau_0 = 2$ and Doppler parameter $b = 10\text{ km s}^{-1}$.

^bRest equivalent width for the column density in column 4.

^cMetallicity assuming the column density in column 4 and $\log N_{\text{HI}} = 22$.

3. High precision measurements, absolute or relative, will be very difficult to achieve. Meaningful constraints that require better than 0.5 dex precision (e.g. nucleosynthetic patterns) may not be attainable. One may, however, be able to distinguish between very high and low dust-to-gas ratios.

4. Aim for the highest spectral resolution at the cost of high signal-to-noise. The only convincing argument that a line is unsaturated is to reconstruct the optical depth profile.

5. Place upper limits on the metallicity using very weak transitions and/or trace elements. Table 2 provides a list of weak transitions for abundant elements (e.g. Fe, Si, O) and stronger transitions of trace elements (e.g. Ge, B). The Table also lists the column density corresponding to a line-profile which is modestly saturated ($\tau_0 = 2$) for a Doppler parameter $b = 8\text{ km s}^{-1}$. If one can establish an upper limit (ideally 3σ including continuum uncertainty) to the equivalent width which is below the corresponding W_λ value (Column 5) then one places an upper limit to the metallicity listed in Column 6, assuming solar relative abundances and ignoring differential depletion. In general, this will require observations with rest equivalent width error $\sigma(W_\lambda) < 30\text{ m\AA}$.

5. CONCLUDING REMARKS

Before concluding, we wish to briefly comment on the abundance measurements for the ISM of GRB presented in the literature. Table 3 summarizes the results to date. The last two columns give the minimum and maximum metallicity values allowed by the data as reported in the literature⁵. One notes that solar (and even super-solar) abundances are allowed in nearly every case. It is evident from Table 3 that the principal conclusion of Savaglio, Fall & Fiore (2003) – GRB sightlines have extreme metal column densities – may be a remarkable understatement. We also caution that the common conclusion that GRB occur in a metal-poor ISM ($[M/H] \leq -1$) may need serious revision.

It is unfortunate that there are few transitions for mild or non-refractory elements that are weak enough to place meaningful upper limits to the abundances; the Zn and Si abundances, for example, are compromised by their relatively strong transitions. We expect, however, that an analysis of the lines listed in Table 2 may improve the constraints (Prochaska *et al.* 2006) and provide more realistic metallicity measurements for the gas within GRB host galaxies.

The authors wish to recognize and acknowledge the very significant cultural role and reverence that the summit of Mauna Kea has always had within the indigenous Hawaiian community. We are most fortunate to have the opportunity to conduct observations from this mountain. J.X.P. thanks E. Jenkins, H.-W. Chen, and J.S. Bloom for valuable discussions and comments on a draft of this manuscript. J.X.P. is partially supported by NASA/Swift grant NNG05GF55G.

REFERENCES

- Barth, A. J. *et al.* 2003, *ApJ (Letters)*, 584, L47.
 Berger, E. *et al.* 2005, *ArXiv Astrophysics e-prints*.
 Castro, S. *et al.* 2003, *ApJ*, 586, 128.
 Chen, H.-W. *et al.* 2005, *ApJ*, 634, L25.
 Crutcher, R. M. 1975, *ApJ*, 200, 625.
 Dessauges-Zavadsky, M. *et al.* 2003, *MNRAS*, 345, 447.
 Fiore, F. *et al.* 2005, *ApJ*, 624, 853.
 Foley, R. J. *et al.* 2005, *ArXiv Astrophysics e-prints*.
 Fynbo, J. P. U. *et al.* 2002, in *Lighthouses of the Universe: The Most Luminous Celestial Objects and Their Use for Cosmology* Proceedings of the MPA/ESO/, p. 187, ed. M. Gilfanov, R. Sunyaev, and E. Churazov, 187.
 Fynbo, J. P. U. *et al.* 2006, *ArXiv Astrophysics e-prints*.
 Gehrels, N. *et al.* 2004, *ApJ*, 611, 1005.
 Gehrels, N. 2006, in press
 Hill, G. *et al.* 2005, *GRB Circular Network*, 4255, 1.
 Howk, J. C., Savage, B. D., and Fabian, D. 1999, *ApJ*, 525, 253.
 Jenkins, E. B. 1986, *ApJ*, 304, 739.
 Jenkins, E. B., Savage, B. D., and Spitzer, L. 1986, *ApJ*, 301, 355.
 Kawai, N. *et al.* 2006, *Nature*, 440, 184.
 Kulkarni, S. R. *et al.* 1999, *Nature*, 398, 389.
 Mirabal, N. *et al.* 2002, *ApJ*, 578, 818.
 Nachman, P. and Hobbs, L. M. 1973, *ApJ*, 182, 481.
 Oke, J. B. *et al.* 1995, *PASP*, 107, 375.
 Prochaska, J. *et al.* 2006, *ApJS*, submitted
 Prochaska, J. X., Chen, H.-W., and Bloom, J. S. 2006, *ArXiv Astrophysics e-prints*.
 Prochaska, J. X., Herbert-Fort, S., and Wolfe, A. M. 2005, *ApJ*, 635, 123.
 Prochaska, J. X. and Wolfe, A. M. 1996, *ApJ*, 470, 403.
 Prochaska, J. X. *et al.* 2001, *ApJS*, 137, 21.

- Savaglio, S. and Fall, S. M. 2004, *ApJ*, 614, 293.
 Savaglio, S., Fall, S. M., and Fiore, F. 2003, *ApJ*, 585, 638.
 Savaglio, S. *et al.* 2004, *ApJ*, 602, 51.
 Spitzer, L. and Jenkins, E. B. 1975, *ARA&A*, 13, 133.
 Spitzer, L. J. and Fitzpatrick, E. L. 1995, *ApJ*, 445, 196.
 Turnshek, D. A. *et al.* 2005, *ArXiv Astrophysics e-prints*.
 Unsöld, A., Struve, O., and Elvey, C. T. 1930, *Zeitschrift fur Astrophysik*, 1, 314.
 Vogt, S. S. *et al.* 1994, in *Proc. SPIE Instrumentation in Astronomy VIII*, David L. Crawford; Eric R. Craine; Eds., Volume 2198, p. 362, 362.
 Vreeswijk, P. M. *et al.* 2004, *A&A*, 419, 927.
 Vreeswijk, P. M. *et al.* 2006, *A&A*, 447, 145.
 Watson, D. *et al.* 2005, *ArXiv Astrophysics e-prints*.
 Wilson, O. C. 1939, *ApJ*, 90, 244.

⁵We will ignore (for the time being) the fact that Zn is a trace element and that a large Zn/H ratio does not require a high gas metallicity.

TABLE 3
SUMMARY TABLE OF ABUNDANCE MEASUREMENTS IN LOW-RESOLUTION GRB SPECTRA

GRB	z	$\log N_{\text{HI}}$	$[\text{M}/\text{H}]_{\text{lit}}^a$	Ref	Instr	Line ^b _{weak}	$W_\lambda(\text{\AA})$	$[\text{M}/\text{H}]_{\text{min}}^c$	$[\text{M}/\text{H}]_{\text{max}}^d$
990123	1.600	22	$-0.7^{+0.05}_{-0.05}$	1,2	Keck/LRIS	Zn II 2026	0.485 ± 0.038	-0.95	—
000926	2.038	21.3 ± 0.25	$-0.15^{+0.05}_{-0.05}$	2,3,4	Keck/ESI	Zn II 2026	0.90 ± 0.1	-0.25	—
010222	1.477	22	$-1.0^{+0.07}_{-0.07}$	5,2	Keck/ESI	Zn II 2026	0.91 ± 0.1	-1.0	—
011211	2.142	20.4 ± 0.2	$-0.9^{+0.6}_{-0.4}$	6,2	VLT/FORS2	Zn II 2026	0.91 ± 0.1	-1.0	—
020813	1.255	22	$-1.1^{+0.06}_{-0.06}$	7,2	Keck/LRIS	Zn II 2026	0.61 ± 0.1	-1.2	—
030323	3.372	21.9 ± 0.07	$-1.3^{+0.20}_{-0.20}$	8	VLT/FORS2	Zn II 2026	0.82 ± 0.09	-0.9	+0.5
050401	2.899	22.5 ± 0.3	$-0.8^{+0.4}_{-0.4}$	9	VLT/FORS2	Zn II 2062		-1.0	—
050505	4.275	22.05 ± 0.1	-1.2	10	Keck/LRIS	Fe II 1611	0.54 ± 0.05	-1.0	—
050904	6.296	21.3 ± 0.2	-1	11	Subaru/FOCAS	S II 1253	0.5 ± 0.15	-1.4	—
060206	4.048	20.85 ± 0.1	$-0.84^{+0.1}_{-0.1}$	12	WHT/ISIS	S II 1250		-1.0	-0.5

^aMetallicity reported in the literature. For those sightlines without N_{HI} measurements, we adopt a reasonably conservative value of 10^{22} cm^{-2} . Note that the errors reported reflect only the uncertainty in the reported metal abundance to highlight the overly optimistic results.

^bMost constraining transition for a metallicity measurement, generally derived from a weak transition. Note that we have not corrected for Mg I blending with the Zn II 2026 transition. This could reduce the metallicity limit by as much as 0.2 dex.

^cMinimum metallicity derived from assuming the transition in Column 8 is optically thin.

^dMaximum metallicity based on the non-detection of a transition or the accurate measurement of an unsaturated transition.

References. — 1: Savaglio, Fall & Fiore (2003); 2: Kulkarni *et al.* (1999); 3: Fynbo *et al.* (2002); 4: Castro *et al.* (2003); 5: Mirabal *et al.* (2002); 6: Vreeswijk *et al.* (2006); 7: Barth *et al.* (2003); 8: Vreeswijk *et al.* (2004); 9: Watson *et al.* (2005); 10: Berger *et al.* (2005); 11: Kawai *et al.* (2006); 12: Fynbo *et al.* (2006)